THE CRYPT CYCLE

Crypt and Villus Production in the Adult Intestinal Epithelium

JOHN TOTAFURNO, MATTHEW BJERKNES, AND HAZEL CHENG
Department of Anatomy, Medical Sciences Building, University of Toronto, Toronto, Ontario, Canada M5S 1A8

ABSTRACT We propose a model for the growth of individual crypts that is able to account for the observed changes in the number of cells in crypts under normal conditions, after irradiation, and after 30% resection. Parameter values for this model are estimated both for mouse and man, and detailed predictions of crypt growth rates are made. This model does not predict a steady-state crypt size; rather it suggests that crypts grow until they bifurcate. We therefore propose a crypt cycle (analogous to the cell cycle) and present evidence that most if not all crypts in the adult mouse are cycling asynchronously and independently. This evidence consists of four experiments that indicate that branching crypts are randomly distributed over the intestinal epithelium, that the plane of bifurcation of branching crypts is randomly oriented with respect to the villus base, and that the size distribution of crypts is consistent with an expanding crypt population. We also report for the first time evidence of villus production in the adult mouse intestinal epithelium. We conclude that the crypt and villus populations in the adult mouse are not in a steady state.

I. INTRODUCTION

The mammalian intestinal epithelium is in a constant state of flux: new cells are continuously produced in the crypts, move to the villi, and eventually are lost into the intestinal lumen. In fact, in the adult mouse, the turnover time for the entire epithelial cell population is ~60 h (Cheng and Bjerknes, 1982, 1983). Thus in terms of the cells that comprise the crypts and villi, the intestinal epithelium is a highly dynamic system.

In contrast, in terms of the crypts and villi themselves, the intestinal epithelium appears essentially static over the 60-h epithelial turnover time. This is because the tissue is in an approximate steady state with cell loss roughly matching cell production (Bjerknes, 1986). Is this static view of the crypt and villus structure of the adult mouse intestinal epithelium acceptable over time scales of the order of weeks or months? We argue that it is not. Instead we propose that continual production of crypts and villi is a normal by-product of cell renewal in the adult intestinal epithelium.

The dynamic nature of the crypt population in adult mice is suggested by the following observations: (*a*) The intestine as a whole grows in size with increasing mouse age and weight (O'Connor, 1966). The number of crypts per villus increases with age also (Cheng and Bjerknes, 1985). (*b*) Approximately 3–10% of crypts are in the process of branching (Maskens and Dujardin-Loits, 1981; Bjerknes, 1986; Cheng and Bjerknes, 1985). Branching crypts are thought to be responsible for crypt production in growth and repair (Cairnie and Millen, 1975). (*c*) Recent in vivo experiments have shown that crypts actively divide with a doubling time of ~107 d (Bjerknes, 1986). (*d*) In any region of the adult small intestine, crypt and villus size vary considerably (Bjerknes and Cheng, 1981*e*, Figs. 13–16 and p. 570; see also Experiment 4 below).

These observations indicate that the number of crypts in the adult is increasing, and new crypts are being produced by crypt bifurcation. We have therefore proposed that crypts are cycling through a division cycle analogous to the cell cycle (Bjerknes, 1986; Cheng et al., 1986*a,b*). In this paper we show how a simple model of crypt cell dynamics implies the necessity of a crypt cycle and report the results of five experiments that test for some of the consequences of such a crypt cycling scenario.

II. A MODEL OF CRYPT GROWTH

In this section we develop a simple model of crypt growth. The rate of growth of the crypt is determined by the cell production rate and the flux of cells out of the crypt. Cell death in the crypt is assumed to be negligible.

(a) The Growth Zone

Cell production occurs in roughly the lower two-thirds of the crypt (Fig. 19.1 of Wright and Alison, 1984; Table 2 of Bjerknes and Cheng, 1981*d*). We have observed that there is usually a narrowing in the upper one-third of the crypt. We call the narrowest point in the upper part of the crypt the "waist" of the crypt (see Fig. 1). The waist is an

Correspondence should be sent to Dr. Bjerknes.

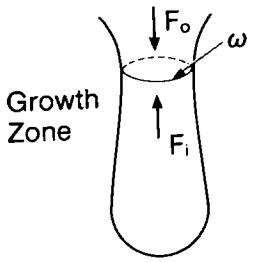

FIGURE 1 Outline of a crypt showing the waist with perimeter ω. Below the waist is the growth zone. As explained in Section IIc, the regions above and below the waist are associated with the forces F_o and F_i, respectively.

identifiable point that apparently lies above the region of cell proliferation. We assume that the waist is the major "bottleneck" to cell loss from the crypt. It is at this point that the flux[1] of cells out of the crypt is a maximum. We will refer to the region from the base of the crypt to the waist as the "growth zone" (not to be confused with the term "proliferative zone" [Fig. 2 of Cairnie et al., 1965]). The growth zone includes all of the cycling cells of the crypt and some of the noncycling cells.

(b) Cell Production

Let the total number of cells in the growth zone be denoted by $n = c + q$, where c and q are the number of cycling and noncycling cells in the growth zone, respectively. In Appendix A we show that under simple assumptions, if there were no loss from the crypt then the growth rates of the cycling and noncycling populations are given by

$$\frac{dc}{dt} = kc \tag{1}$$

and

$$\frac{dq}{dt} = k\rho c, \tag{2}$$

where k and ρ are constants. (Eqs. A16 and A17 of Appendix A relate k and ρ to the cell cycle time, τ, and to the average number of stem cells produced when a stem cell divides, α). Adding Eqs. 1 and 2 and integrating Eq. 1 to obtain $c(t)$ yields

$$\text{Total cell production rate} \left(\frac{dn}{dt} \text{ in absence of loss}\right) = k'c_o e^{kt}, \tag{3}$$

where $k' = k(\rho + 1)$ and where $c_o > 0$ is the number of proliferative cells at $t = 0$.

(c) Cell Loss

By definition, loss from the growth zone is due to noncycling cells that move past the waist into the upper part of the crypt. The inclusion of cell loss from the growth zone, therefore, changes Eq. 2 to read

$$\frac{dq}{dt} = k\rho c - \Phi\omega, \tag{4}$$

where Φ is the flux of cells through the waist in units of number of cells per unit length of perimeter and ω is the perimeter of the waist. This approach to the loss of cells from the growth zone is reasonable as long as the growth fraction below the waist (i.e., c/n) < 1. Otherwise, if the growth fraction equaled one, cycling cells would be lost and the model would be ill-defined.

The dependence of the flux of cells (given by Φ) upon the number of cells in the growth zone is obtained as follows. Since crypt renewal is slow compared with the cell cycle time τ, we assume that cell volume is constant. We then assume that cell flow can be modeled as the flow of an incompressible fluid. The waist separates the growth zone and the top of the crypt. Each of these two regions is associated with a force that causes the cells of the region to move: the force causing cells at the waist to move out of the growth zone is denoted by F_i, and the force on cells at the waist that tends to resist the movement of cells out of the growth zone is denoted by F_o (see Fig. 1). The flux of cells through the waist is assumed to be proportional to the difference in these forces, i.e.,

$$\Phi = \xi(F_i - F_o), \tag{5}$$

where $\xi > 0$ is a constant.

Since F_o is associated with all of the epithelium outside of the growth zone of a given crypt, it presumably changes slowly relative to the time scale of crypt branching and, therefore, can be taken to be constant. To derive F_i from first principles goes beyond the scope of this paper and the empirical data (to do so would require the viscoelastic properties of the crypt cells and the underlying basement membrane). We assume that F_i is a linear function of n. Substituting F_o and F_i into Eq. 5 yields for the flux

$$\Phi = \sigma n + \phi, \tag{6}$$

where σ is the flux per cell driven by the presence of other cells in the growth zone, and ϕ is the "walking" flux due to interaction of the cells with the basement membrane.

We assume on dimensional grounds that the waist perimeter, ω, is proportional to $v^{1/3}$, where v is the volume of the growth zone. Now $v = \bar{v}n$, where $\bar{v}$ is the average volume of a crypt cell (plus the associated portion of the crypt lumen). Therefore,

$$\omega = \Gamma n^{1/3}, \tag{7}$$

where $\Gamma > 0$ is a constant. We will see that Eq. 7 is consistent with observation.

Using Eqs. 6 and 7, we conclude that the

$$\text{Cell loss rate} = \Phi\omega \simeq \Gamma n^{1/3}(\sigma n + \phi). \tag{8}$$

(d) Growth Equations

Collecting our assumptions, the model of crypt growth outlined above is determined by the equations

[1]Defined as the number of cells per unit time per unit length.

$$\frac{dc}{dt} = kc, \tag{1}$$

and

$$\frac{dq}{dt} = k\rho c - \Gamma n^{1/3}(\sigma n + \phi). \tag{9}$$

Thus (see Eq. 3)

$$\frac{dn}{dt} = k'c - \Gamma n^{1/3}(\sigma n + \phi)$$

$$= \frac{k'}{s}(sc_0 e^{kt} - n^{4/3} - rn^{1/3}), \tag{10}$$

where s and r are two positive dimensionless constants defined as

$$s = k'/\sigma\Gamma \tag{11}$$

and

$$r = \phi/\sigma. \tag{12}$$

By solving Eq. 10, the total number of cells in the growth zone as a function of time, $n(t)$, can be determined.

The crypt growth dynamics determined by Eq. 10 does not possess a stable equilibrium. The rate of growth dn/dt is not identically zero for any n (except when n and $c_0 = 0$) because of the continual growth of the proliferative cell population (cf., Eq. 1). Assuming that individual crypts have some upper size limit, the absence of a steady-state crypt size in the model makes crypt bifurcation and hence a crypt cycle a necessity. As the crypt grows, its growth fraction changes but we will see that in practice this variation is within reasonable limits. In Appendix C we discuss the consequences of holding the growth fraction in the model fixed.

III. MATERIALS AND METHODS

(a) Analysis of Crypt Growth Model

Eq. 10 was solved numerically for $n(t)$ using values for the parameters k', c_0, s, and r corresponding to normal adult mouse jejunum and to human sigmoid colon. Estimates for the values of these parameters are given in Table I. Published data were used to estimate k' (see Appendix A) and c_0 (see Appendix B). Ranges for the values of s and r were chosen so that the solution of Eq. 10 would be simultaneously consistent with the measured crypt replication time, T, and with the time it takes for the crypt to empty after all of its stem cells are killed (see Appendix B). The growth fraction as a function of the age of the crypt was computed. The form of Eq. 7 was tested using data obtained as described in Section IIIe, *ii*. To test the generality of the model, $n(t)$ was also computed for mouse jejunum after 30% resection using parameters derived from those already determined for normal mouse jejunum.

(b) Experiment 1: Distribution of Branching Crypts

(i) Theory. The crypt growth model illustrates a mode of growth leading to crypt cycling. We wish to determine if all crypts cycle and if they cycle asynchronously and independently. This would imply that cycling crypts are dispersed uniformly over the intestinal epithelium as opposed to occurring in clusters. If we assume the above conditions, the number of branching crypts k attached to a villus with a total of n attached crypts would approximately follow the binomial distribution

$$\binom{n}{k} q^k (1 - q)^{n-k}, \tag{13}$$

where q is the probability that any single crypt is in the process of branching at the time of sampling. Here q is estimated by the fraction of crypts in the population as a whole that are branching at the time of sampling. In this experiment we check if the probability distribution of branching crypts corresponds to Eq. 13.

(ii) Experimental. Intact epithelial sheets from 3-cm long segments of proximal jejunum starting 1 cm from the ligament of Treitz from eight male Swiss albino mice (30–35 g) were isolated by the EDTA perfusion method of Bjerknes and Cheng (1981*e*). The epithelium was vibrated into 3.5% glutaraldehyde in saline and fixed for 30 min. The preparation results in epithelial sheets with villi and crypts intact.

The isolated epithelial sheets were cut into small pieces with 20–50 villi each. 50 pieces from each animal were randomly chosen. From each piece a single villus was randomly selected. Both the total number of crypts and the number of branching crypts surrounding the selected villus were counted. Each branching crypt was scored as one crypt. Thus, both the number of crypts and the number of branching crypts connected to a total of 400 villi were obtained.

In comparing the data with Eq. 13, villi with different numbers of connected crypts n were treated as separate groups. A chi-square test was performed to compare the expected distribution with the data from each group. To get an overall measure of the goodness of fit of the model, the individual P-values from the chi-square tests were combined by summing the logarithm of the P-values and multiplying the sum by -2. This variable is approximately chi-square distributed with the number of

TABLE I
CRYPT GROWTH MODEL PARAMETERS*

	k'	c_0	s	r	Γ	$\sigma \times 10^{-4}$	ϕ	n_i	n_f	T	γ	$\bar{v}$
	h^{-1}				μm	$h^{-1}\,\mu m^{-1}$	$h^{-1}\,\mu m^{-1}$			d	%	μm^3
Mouse jejunum (group A)	0.0768	195	13.3–12.34‡	128–82‡	19.6	2.95–3.18‡	0.0378–0.0261‡	217	517	107	90	800
Human sigmoid colon	0.0139	360	32.6–31.9‡	128–82‡				600	1,800	4,380	60	
Mouse jejunum after 30% resection	0.0765	303–308‡	13.2–12.29‡	128–82‡	19.6	2.96–3.18‡	0.0379–0.0261‡	312	744	33		

*See Sections II, IIIa, and IVa and Appendices A and B for definitions and manner of determination. s is the parameter given in Eq. 10 (not the number of stem cells).

‡Ranges shown are ordered to correspond to from 5 to 25% of the cells of the crypt assumed killed after irradiation, as described in Appendix B.

degrees of freedom equal to twice the number of individual chi-square tests being combined (Fisher, 1970).

(c) Experiment 2: Distribution of Branching Crypts about Villi

(i) Theory. In this experiment we consider another consequence of the proposal that all crypts cycle independently and asynchronously. Consider villi with two branching crypts. The placement of these branching crypts about a given villus can be characterized by the minimum number of nonbranching crypts associated with the villus that separate the pair of branching crypts. If all crypts cycle independently in asynchronous fashion (see Experiment 3 and Discussion), then all possible spatial distributions of the two branching crypts about villi with n crypts are equally likely. For example, a villus with a total of seven connected crypts, two of which are branching, could have the branching crypts separated by 0, 1, or 2 nonbranching crypts (see Fig. 2). Each of these spatial distributions of branching crypts is equally likely. In general, the probability of a separation by j nonbranching crypts on a villus with a total of n attached crypts, two of which are branching, is

$$P(j|n) = \begin{cases} \dfrac{1}{[\![n/2]\!]}, & n \text{ odd and } 0 \le j \le ([\![n/2]\!] - 1) \\ \dfrac{2}{(n-1)}, & n > 2 \text{ and even and } 0 \le j < \left(\dfrac{n}{2} - 1\right) \\ \dfrac{1}{(n-1)}, & n \text{ even and } j = \left(\dfrac{n}{2} - 1\right) \\ 0, & \text{otherwise} \end{cases} \tag{14}$$

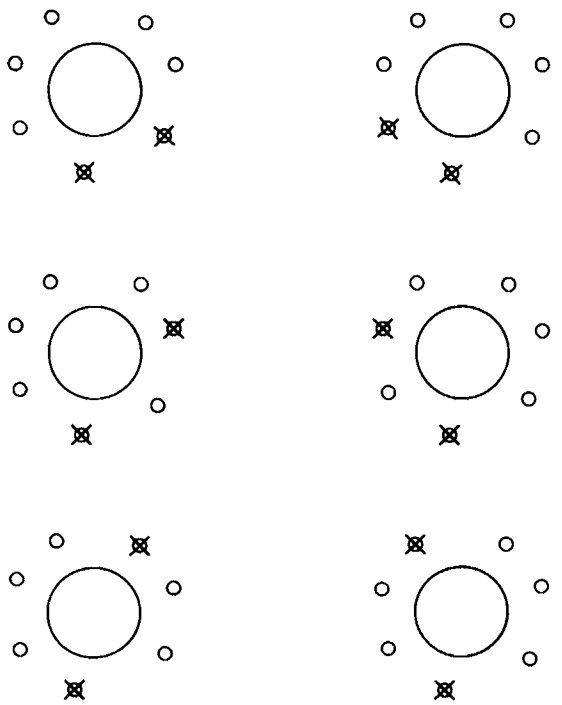

FIGURE 2 The possible spatial distributions of a pair of branching crypts about a villus connected to seven crypts. The base of the villus is represented by the large circle; the top of the crypts are represented by the smaller circles. Crypts in the process of branching are marked by an "×."

where $[\![n/2]\!]$ represents the greatest integer $\le n/2$. The expected number of villi with a given separation between branching crypts, j, is simply the sum over all n of $mP(j|n)$ where m is the number of villi with n crypts attached.

(ii) Experimental. Intestinal epithelial sheets were prepared as described in Experiment 1. A total of 50 villi were chosen, each of which was connected to two branching crypts. The minimum number of nonbranching crypts that separated the branching crypts was counted (see Fig. 2). This minimum separation and the total number of crypts connected to the villus were recorded. Comparison of these results to the model Eq. 14 was performed using a chi-square test.

(d) Experiment 3: Orientation of Branching Crypts

In Experiments 1 and 2, asynchrony of the crypt cycle was tested. A contributing source of this lack of synchrony is if neighboring crypts surrounding a villus are not necessarily siblings. Presumably they would not always be siblings if the plane of division of a branching crypt is randomly oriented with respect to the neighboring portion of the base of the villus to which it is connected. In this experiment we test, therefore, whether or not the division plane is randomly oriented with respect to the villus.

The tissue used in Experiment 1 was also used in this experiment. Villi connected to at least one branching crypt were selected. Cross-sections through the bases of each of these villi and of the crypts surrounding them were traced using a drawing tube and the positions of the tops of the crypts were marked. For each branching crypt, the angle between the long axis of the associated villus base and the line perpendicular to the division plane of the branching crypt was measured from the drawings. The angular data for those branching crypts located near the ends of the long axes of the villus bases was analyzed separately from the angular data for those branching crypts located nearer the middle of the long axes. A total of 108 branching crypts near the end of the long axes of the villus cross-sections and 92 nearer the middle was used. The uniformity of the distribution of measured angles in each of these classes was tested using both the chi-square and the nonparametric Kolmogorov–Smirnov statistic (Sokal and Rohlf, 1981).

(e) Experiment 4: Distribution of Crypt Volumes

(i) Theory. Under the assumptions that all crypts cycle independently and asynchronously with the same average crypt cycle time, T, and with insignificant crypt loss,[2] the cycling of crypts expected on the basis of the crypt growth model leads to exponential growth in the crypt population of the form

$$N(t) \simeq N_0 \exp(t \ln 2/T), \tag{15}$$

where N_0 is the number of crypts at time $t = 0$. This in turn implies a probability distribution for the age of the crypts of the form

$$f(\varphi) = \frac{2 \ln 2}{T} \exp\left(-\frac{\ln 2}{T}\varphi\right), \tag{16}$$

[2]Observation of 328 crypts over the period of 3 wk revealed no crypt loss (Bjerknes, 1986). Using the conservative value of a possible 1% crypt loss over 3 wk (see Bjerknes, 1986) and assuming that crypt loss is proportional to the number of crypts (Steel, 1968), the half-life for crypt loss would be >207 wk. The rate of crypt loss is, therefore, much less than the rate of crypt production with its doubling time of ~15 wk (Bjerknes, 1986).

where φ is the time since division, i.e., φ is the age of the crypt so that $0 \leq \varphi < T$ (cf. Steel, 1968).

Assuming that the volume of a crypt is a steadily increasing function of age $v(\varphi)$, we can rewrite Eq. 16 to obtain the probability distribution of $f(v)$ for the volume of the crypt. In our simple model, the volume v ranges from a minimum V_0 just after division to a maximum $V_0 + \Delta V$ just before the completion of crypt bifurcation. Assuming that the error in measuring a crypt of volume v' is normally distributed about v', the observed probability distribution of crypt volumes is given by

$$p(v) = \int_{V_0}^{V_0+\Delta V} f(v')g(v|v',\sigma)\,dv', \tag{17}$$

where $f(v')$ is the model probability density for volume v', and $g(v|v',\sigma)$ is a normal distribution of volume v about the volume v' with standard deviation σ.[3] In Section IVa it is shown that v is roughly a linear function of φ so that

$$f(v)\,dv = \frac{2 \ln 2}{\Delta V} \exp\left[-\frac{\ln 2}{\Delta V}(v - V_0)\right] dv. \tag{18}$$

Suppose that the fraction of the crypt cycle time spent in budding (initial stage of division) and bifurcation (see Fig. 2 of Cheng et al., 1986*b*) is a. Then (assuming $v(\varphi)$ is linear) budding and bifurcation commence at a volume $V_0 + (1 - a)\Delta V$. Let $p_b(v)$ be the probability density that a randomly chosen crypt is both branching and of volume v. Introducing the coefficient of variation, $CV = \sigma/v'$, and the quantities $\nu = \ln 2(v - V_0)/\Delta V$, $\nu' = \ln 2(v' - V_0)/\Delta V$, and $\beta = CV \ln 2\, V_0/\Delta V$, we obtain

$$p_b(v) = \sqrt{\frac{2}{\pi}} \frac{\ln 2}{\Delta V} \int_{\nu_1'}^{\nu_2'} (CV\nu' + \beta)^{-1} \exp\left\{-\frac{1}{2}\left(\frac{\nu - \nu'}{CV\nu' + \beta}\right)^2 - \nu'\right\} d\nu', \tag{19}$$

where $\nu_1' = (1 - a) \ln 2$ and $\nu_2' = \ln 2$. Similarly the probability density that a randomly chosen crypt is both nonbranching and of volume v, $p_{nb}(v)$, is given by a similar equation with $\nu_1' = 0$ and $\nu_2' = (1 - a) \ln 2$. With these definitions,

$$p(v) = p_b(v) + p_{nb}(v). \tag{20}$$

As shown in Fig. 3, as CV increases, the underlying exponentially decaying probability distribution for the crypt volumes given by $f(v)$ (see Eq. 18) broadens.

(ii) Experimental. Two lots (A and B) of five male Swiss albino CD-1 mice each were used in this study. The five animals in each group were raised under similar conditions and were of similar age and weight (28.5–29.5 g for group A and 32–33.7 g for group B). Isolated epithelial sheets from proximal jejunum of each animal were cut into small strips. Longitudinal outlines of the individual crypts in each strip were made using a drawing tube (magnification 490). All crypts in each strip were traced. A total of 364 crypts in group A were traced, of which 14 were judged from the traced outlines to be branching. In group B, 319 crypts were traced, 22 of which were judged to be in the process of branching.

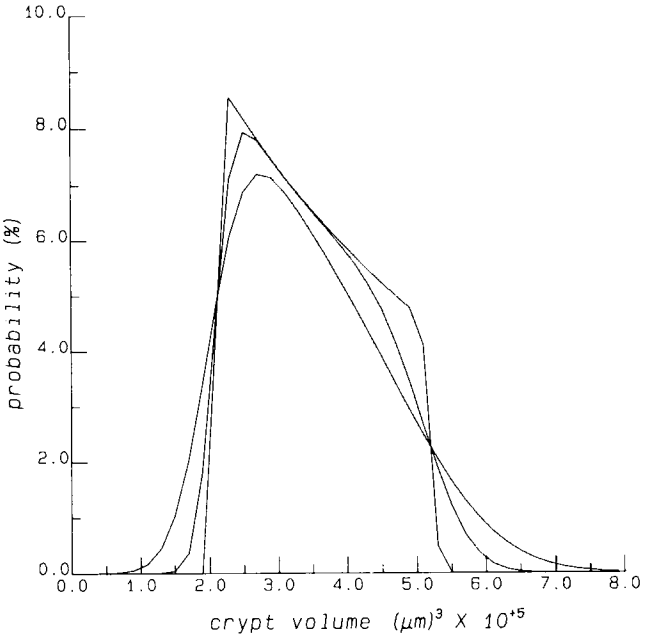

FIGURE 3 The probability distribution p for crypt volumes v as given by Eq. 20 for several values of the coefficient of variation CV. Here $V_0 = 2.1 \times 10^5\ \mu m^3$ and $\Delta V = 3.1 \times 10^5\ \mu m^3$.

From the crypt outlines, the volume of each crypt was estimated in the following way. Crypts were assumed to be rotationally symmetric about their longitudinal axis. The volume of the crypt could, therefore, be estimated on the basis of a longitudinal two-dimensional projection once the symmetry axis of the outline was chosen. Equivalent points on either side of the symmetry axis ideally should be equidistant from the axis. The computer algorithm used to select the symmetry axis therefore chooses that axis for which the sum of the squared differences in the distance of equivalent points from the axis is a minimum. The algorithm chose a reasonable symmetry axis (or axes in the case of bifurcating crypts) for 342 of the 364 crypts in group A (94%) and for 291 of the 319 crypts of group B (91%). It was assumed that no bias in the results was introduced by not using the small percentage of crypts whose symmetry axis was not able to be determined by the algorithm.

Once the symmetry axis was chosen, the volume of revolution of the crypt outline was determined. An estimate of the precision of the volume measurement was obtained by measuring the volume of a single crypt using several different projections of the same crypt. This was done for each of a total of nine crypts to determine how the precision of the crypt volume measurement varied with crypt volume. For both groups A and B, a maximum likelihood fit of $p(v)$ (see Eq. 20) to the measured crypt volumes was performed and then the expected probability densities $p(v)$, $p_b(v)$, and $p_{nb}(v)$ were compared with the data using the chi-square test.

In addition to the volume, the width of the narrowest point in the top part of the crypt, i.e., the waist of the crypt (see Fig. 1), was measured from the outlines of the crypts. The relationship of waist diameter to crypt volume is reported in Section IVa in conjunction with the model of crypt growth.

(f) Experiment 5: Search for Villus Production

Given that crypts are continuously produced in the adult, it seems reasonable to expect that the villus population is also growing. A careful

[3]Since volumes are strictly positive, the normal distribution is a useful model for the error only if $g(v|v',\sigma)$ is small for $v < 0$ and $V_0 \leq v' \leq V_0 + \Delta V$. It is sufficient to require that

$$\int_{-\infty}^{0} g(v|V_0,\sigma) = \frac{1}{2}\,\mathrm{erfc}\left(\frac{V_0}{\sigma\sqrt{2}}\right) = \frac{1}{2}\left[1 - \mathrm{erf}\left(\frac{V_0}{\sigma\sqrt{2}}\right)\right],$$

(see Abramowitz and Stegun, 1965) be small. Since $\mathrm{erf}(3) = 0.999978$, we require $V_0/\sigma\sqrt{2} \gtrsim 3$ which implies that σ/V_0 be less than ~24%.

search was made, therefore, of the isolated epithelial sheets (obtained in Experiment 1) for evidence of new villus formation. Occasionally, a single ring of crypts surrounding two villi was observed. Often one of the pair of villi was very small (see Fig. 4). The number of crypts associated with these villus pairs was recorded as was the number of attached branching crypts (as in Experiment 1).

IV. RESULTS

(a) The Crypt Growth Model

The predicted number of cells in the growth zone as a function of time, $n(t)$, is shown in Fig. 5 for the mouse jejunum (group A) and in Fig. 6 for human sigmoid colon. The figures show the growth curves for the values of s and r at the extremes of the estimated range. The dynamics of the model is such that crypt growth is relatively insensitive to the initial size of the crypt n_i; the growth curve quickly approaches that intrinsically set by the choice of k', s, and r. The growth fraction of the growth zone is found for most of the crypt cycle to be in the range 69–76% for the mouse jejunum and in the range 34–40% for the human sigmoid colon (corresponding to a growth fraction for the crypt as a whole of ~46–51% and 17–20%, respectively). Of particular significance to us is that $n(t)$ can be roughly approximated by a straight line, justifying our use of a linear map between crypt volume v and age (Section IIIe, *i*). In obtaining these growth curves, we assumed that the stem cell pool grows to twice its initial size in the crypt replication time, T (see Appendix A). Provided the process of crypt branching distributes the stem cells equally to the daughter crypts, the growth shown can be repeated for each daughter crypt. In this way a stable crypt replication cycle can be established.

FIGURE 4 Villi and crypts of an isolated section of mouse intestinal epithelium. The arrow points to a villus which is much smaller than its neighbors presumably indicating villus production in the adult.

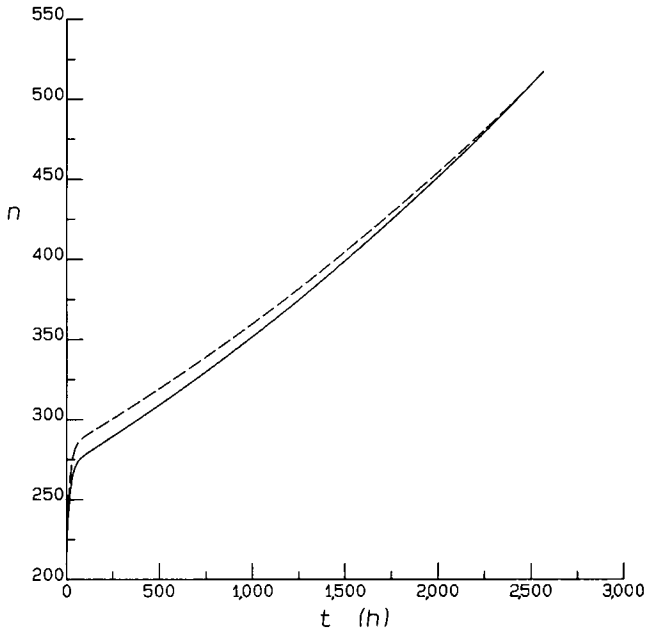

FIGURE 5 Number of cells n in the growth zone as a function of crypt age t for mouse jejunum. The curves are solutions of Eq. 10 with parameters as given in Table I. The solid curve is for the largest allowed s and r values; the dashed line for the smallest.

The equation $w = aV^b$, where w is the width of the crypt waist, V is the total volume of the crypt, and a and b are fitted parameters, was found to fit the data with a correlation coefficient of 0.645 ($P < 0.001$, $dF = 324$) (see

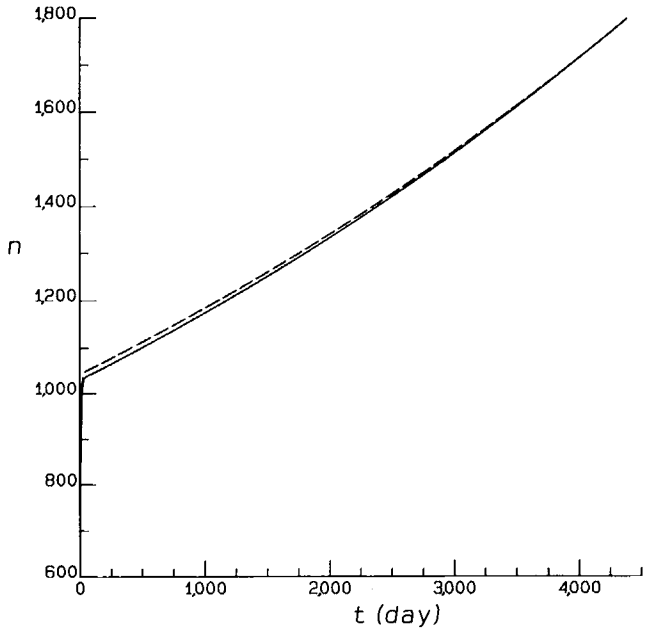

FIGURE 6 Same as Fig. 5 but for human sigmoid colon.

Section IIIe, *ii*). The value $b = 1/3$ lies within the 95% confidence limits on b (range 0.317–0.410), thus affirming the use of the cube root dependence in Eq. 7. Fitting $w = aV^{1/3}$ to the data yielded $a = 0.587$. Now the length of the perimeter of the waist ω is given by $\omega = \pi w$ (assuming axial symmetry). Furthermore, $V = \bar{v} n_{TOT}$, where $\bar{v}$ is the average volume of a crypt cell (plus associated crypt lumen) (see Section IIc) and n_{TOT} is the total number of cells in the crypt which we assume equals $3n/2$ (see Appendix B). Therefore $\omega = \Gamma n^{1/3}$, where $\Gamma = \pi a(3\bar{v}/2)^{1/3} = 19.6\ \mu m$.

As a further test of the model, we investigated its behavior for 30% small intestinal resection. After 30% resection in the mouse small intestine, mean crypt size increases by 44 ± 24% ($\bar{x}$ ± 95% confidence limits), the crypt replication time decreases to $T = 33$ d, and the cell cycle time does not change significantly (see Table 3 in Cheng et al., 1986*b*). Changing k' accordingly, assuming n_i and n_f increase by 44%, but leaving Γ, σ, and ϕ the same as determined for normal mouse jejunum, we found that the model yields the required rate of growth provided the initial number of cycling cells in the crypt, c_o, is increased by between 55 and 58% (for the range of σ from smallest to largest) (see Table I). Since the mean number of cycling cells in a randomly chosen crypt is proportional to c_o (see Eqs. 16 and A11), this predicted increase in c_o (driven by an increase in the number of stem cells) is consistent with the finding that the proliferative compartment expands by approximately the same proportion as the crypt as a whole (i.e., 44 ± 24% in this case) (Bjerknes and Cheng, 1981*d*). Hence the model seems consistent with existing resection data.

(b) Experiment 1: Distribution of Branching Crypts

Associated with the 400 villi sampled were 6,276 crypts of which 134 were branching. The estimated fraction of branching crypts, q, is therefore 0.02135 ± 0.00365 ($\bar{x}$ ± 95% confidence limits). A mean of 15.7 crypts were attached to the sampled villi. Table II lists the values of chi-square obtained in comparing the expected distribution (Eq. 13) with the data both for the groups of villi with different numbers of connected crypts n and for the combined data. No significant difference between the model and the data was indicated by these results ($\chi^2 = 28.9$, $dF = 24$, $P = 0.22$).

(c) Experiment 2: Distribution of Branching Crypts about Villi

In Table III we list the expected number of villi having n connected crypts, two of which are branching, with j crypts separating the branching crypts (given by $m\,P(j|n)$, where m is the number of villi with n crypts, as explained in Section IIIc, *i*) together with the observed number. The comparison of the expected results with those observed is also presented in Table III. The observations were not significantly different from the results expected for randomly distributed crypts ($\chi^2 = 8.89$, $dF = 7$, $P = 0.26$).

TABLE II
NUMBER OF BRANCHING CRYPTS AROUND VILLI

No. of crypts around villus	Branching crypts				χ^2§	dF	P_i
	0	1	2	3			
9	2(1.647)*	0(0.323)	0(0.028)	0(0.001)	‡	‡	‡
10	3(4.029)	2(0.879)	0(0.086)	0(0.005)	‡	‡	‡
11	9(11.042)	3(2.650)	0(0.289)	2(0.019)	1.79	1	0.18
12	15(15.437)	5(4.041)	0(0.485)	0(0.035)	0.05	1	0.82
13	33(28.704)	5(8.140)	0(1.066)	0(0.085)	3.01	2	0.22
14	39(39.919)	15(12.192)	0(1.729)	0(0.151)	2.55	2	0.28
15	44(51.365)	24(16.809)	3(2.567)	0(0.243)	4.14	2	0.12
16	39(40.356)	16(14.086)	1(2.305)	1(0.235)	0.42	2	0.81
17	34(30.487)	10(11.307)	0(1.973)	0(0.215)	2.74	2	0.25
18	22(24.412)	14(9.586)	0(1.778)	0(0.207)	4.26	2	0.12
19	18(15.927)	5(6.602)	0(1.296)	1(0.160)	0.80	2	0.67
20	12(11.041)	5(4.817)	0(0.998)	0(0.131)	1.22	2	0.54
21	3(4.449)	3(2.038)	1(0.445)	0(0.061)	1.30	1	0.26
22	6(4.354)	1(2.090)	0(0.479)	0(0.070)	1.65	1	0.20
23	0(1.217)	2(0.611)	0(0.146)	0(0.022)	‡	‡	‡
24	0(1.191)	2(0.624)	0(0.156)	0(0.025)	‡	‡	‡

*Observed (expected from Eq. 13).
‡Insufficient data for comparison.
§Overall chi-square statistic $\chi^2 = -2\,\Sigma_i \ln P_i = 28.9$ indicates that the model predictions are not significantly different from the data ($P = 0.22$, $dF = 24$).

TABLE III
SEPARATION BETWEEN BRANCHING CRYPTS

No. of crypts connected to villus*	No. of villi*	No. of crypts separating branching crypts (j)*									
		0	1	2	3	4	5	6	7	8	9
n	*m*										
7	1	1/3‡	1/3	1/3							
		(0)	(1)	(0)							
8	1	2/7	2/7	2/7	1/7						
		(1)	(0)	(0)	(0)						
9	5	5/4	5/4	5/4	5/4						
		(1)	(1)	(1)	(2)						
10	9	2	2	2	2	1					
		(2)	(3)	(1)	(1)	(2)					
11	7	7/5	7/5	7/5	7/5	7/5					
		(1)	(1)	(2)	(1)	(2)					
12	6	12/11	12/11	12/11	12/11	12/11	6/11				
		(2)	(1)	(2)	(1)	(0)	(0)				
13	5	5/6	5/6	5/6	5/6	5/6	5/6				
		(3)	(0)	(0)	(0)	(1)	(1)				
14	5	10/13	10/13	10/13	10/13	10/13	10/13	5/13			
		(1)	(0)	(0)	(1)	(3)	(0)	(0)			
15	2	2/7	2/7	2/7	2/7	2/7	2/7	2/7			
		(0)	(1)	(0)	(0)	(1)	(0)	(0)			
16	4	8/15	8/15	8/15	8/15	8/15	8/15	8/15	4/15		
		(1)	(0)	(2)	(0)	(1)	(0)	(0)	(0)		
17	1	1/8	1/8	1/8	1/8	1/8	1/8	1/8	1/8		
		(0)	(0)	(0)	(0)	(1)	(0)	(0)	(0)		
19	3	1/3	1/3	1/3	1/3	1/3	1/3	1/3	1/3	1/3	
		(0)	(0)	(1)	(1)	(0)	(0)	(0)	(0)	(1)	
21	1	1/10	1/10	1/10	1/10	1/10	1/10	1/10	1/10	1/10	1/10
		(1)	(0)	(0)	(0)	(0)	(0)	(0)	(0)	(0)	(0)
Total observed		13	8	9	7	11	1	0	0	1	0
Total expected§		9.34	9.34	9.34	8.86	6.47	3.52	1.76	0.90	0.43	0.10

*Defined in Section IIIc, *i*.
‡Expected from Eq. 14 (observed).
§Chi-square statistic indicates model predictions are not significantly different from the data ($\chi^2 = 8.89$, $P = 0.26$, $dF = 7$).

(d) Experiment 3: Orientation of Branching Crypts

For the class of branching crypts near the end of the long axis of the associated villi, no significant difference between the measured distribution of angles and uniformity was found using both the chi-square test ($\chi^2 = 14.0$, $dF = 17$, $P = 0.67$) and the Kolmogorov–Smirnov test ($D = 0.0556$, $n = 108$) at the 5% level. Similarly for the branching crypts nearer the middle of the villus, the angular distribution was found to be uniform using both the chi-square test ($\chi^2 = 18.7$, $dF = 17$, $P = 0.35$) and the Kolmogorov–Smirnov test ($D = 0.1305$, $n = 92$) at the 5% level. Thus the orientation of the plane of division of branching crypts appears to be distributed randomly with respect to the neighboring portion of the associated villus base.

(e) Experiment 4: Distribution of Crypt Volumes

The results of this experiment are summarized in the plot of the occurrence of crypts as a function of volume shown in Figs. 7 and 8 for groups A and B, respectively.

To determine the dependence of the coefficient of variation on the crypt volume, the estimated standard deviation of five distinct projections for a series of nine crypts was obtained. The standard deviation was found to grow with volume at an approximately constant rate. Thus, in fitting Eq. 20 to the data, the coefficient of variation, *CV*, was assumed to be independent of the volume v'.

The expected probability distribution for crypt volumes, $p(v)$, has three parameters: the minimum crypt volume V_0, the range of crypt volumes ΔV, and the coefficient of variation CV. A maximum likelihood fit of Eq. 20 to the data for the total number of observed crypts as shown in Figs. 7 and 8 using the minimization routine MINUET (C.E.R.N.) yielded the values of the parameters shown in Table IV. For both groups A and B, the maximum volume before the completion of branching, given by $V_0 + \Delta V$, is roughly twice the minimum volume V_0. There was no statistically significant difference between the fits of $p(v)$ and the data for both groups A and B as shown in Figs. 7 and 8, respectively (group A, $\chi^2 = 60.2$, $dF = 58$, $P = 0.40$; group B, $\chi^2 = 38.7$, $dF = 41$, $P = 0.57$).

Both groups A and B show an excess of small crypts as compared with that expected on the basis of the model. However, in the model for the probability distribution of crypt volumes, a constant growth rate for the crypt was assumed. In fact, the crypt growth model indicates that growth rate increases slightly as a crypt becomes larger (see Figs. 5 and 6). This would increase the predicted proportion of smaller crypts.

To compare the occurrence of branching and non-branching crypts to that given by $p_b(v)$ and $p_{nb}(v)$ (see Eq. 19), respectively, the fraction of the crypt cycle spent in budding and bifurcation, a, is required. It can be shown that under the assumption of exponential growth of the crypt population

$$a = \frac{\ln (1 + I)}{\ln 2}, \tag{21}$$

where I is the observed fraction of budding and bifurcating crypts (Cheng et al., 1986*b*). The average branching ratio I for group A was 3.2 ± 0.63% ($\bar{x}$ ± SE), whereas that for group B was 6.9 ± 1.2%. These two branching ratios are significantly different (Student's t test; $P < 0.012$, $dF = 8$). Eq. 21 yields $a = 4.5 \pm 0.9\%$ ($\bar{x}$ ± SE) for group A and $a = 9.6 \pm 1.6\%$ for group B.

Figs. 7 and 8 show for groups A and B, respectively, the expected distribution of branching and nonbranching crypts given by $p_b(v)$ and $p_{nb}(v)$, respectively. Here the same values of V_0, ΔV, and CV obtained in the fit of $p(v)$ to

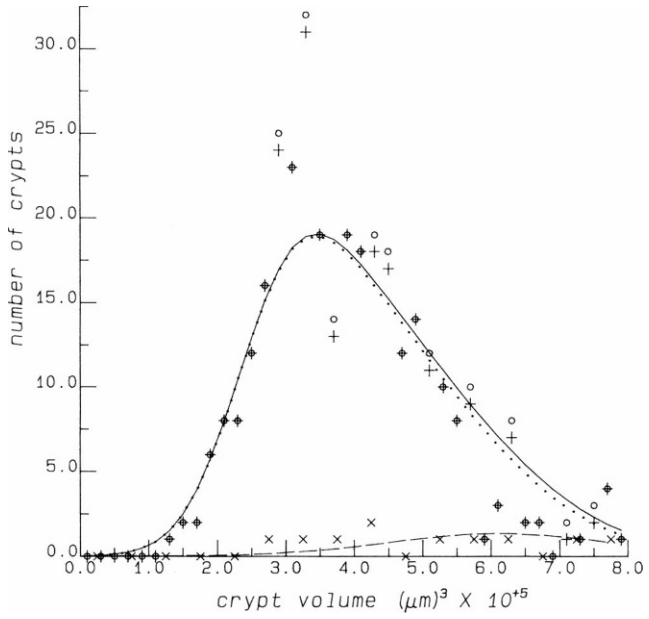

FIGURE 7 The occurrence of mouse jejunal crypt volumes v for group A. A total of 342 crypts (10 of which were branching) were used in the analysis. The mean volume of these crypts was (4.09 ± 0.084) × 10^5 μm³ ($\bar{x}$ ± SE). The measured data are indicated by the symbols; the curves are maximum likelihood fits of the model given by Eqs. 19 and 20 to the data. The ×'s and dashed line correspond to branching crypts, the +'s and dotted line to nonbranching crypts, and the circles and solid line to the pooled branching and nonbranching data. The number of crypts shown are for bins 0.2 × 10^5 μm³ wide in the case of the nonbranching and pooled crypt data and 0.5 × 10^5 μm³ wide in the case of the branching crypt data. The fitted curves had $V_0 = 2.6 \times 10^5$ μm³, $\Delta V = 3.6 \times 10^5$ μm³, and $CV = 0.26$ (see Section IIIe, *i* for description of these parameters). The estimated fraction of the crypt cycle spent branching used in computing the curves was $a = 4.5\%$ (see Eq. 21).

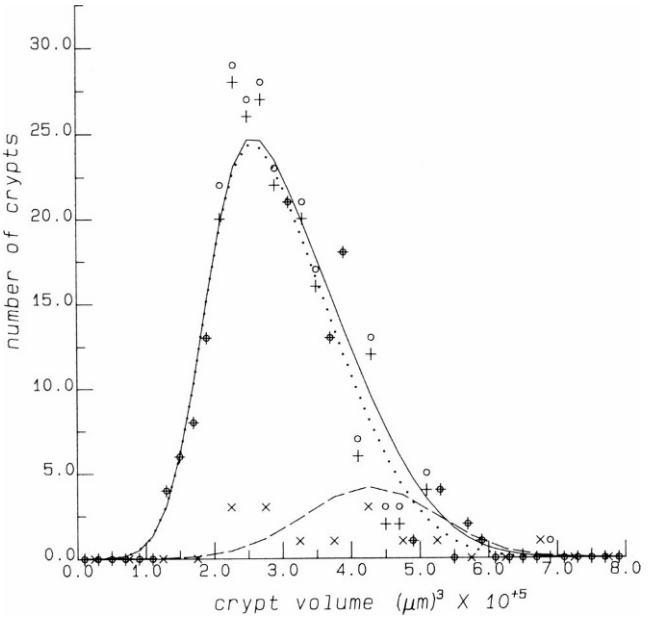

FIGURE 8 Same as Fig. 7 but for the mice of group B. A total of 291 crypts (14 of which were branching) were used in the analysis. The mean volume of these crypts was (3.04 ± 0.058) × 10^5 μm³ ($\bar{x}$ ± SE). Here $V_0 = 2.0 \times 10^5$ μm³, $\Delta V = 2.4 \times 10^5$ μm³, $CV = 0.22$, and $a = 9.6\%$.

TABLE IV
CRYPT VOLUME DISTRIBUTION PARAMETERS*

	Group A	Group B
$V_0 \times 10^5$ μm³	2.6 + 0.4 − 0.3	2.0 ± 0.3
$\Delta V \times 10^5$ μm³	3.6 + 0.8 − 0.9	2.4 + 0.6 − 0.8
CV	0.26 + 0.06 − 0.05	0.22 + 0.06 − 0.05

*Maximum likelihood fit of parameters in Eq. 20; 95% confidence limits are shown.

the data were used. There was no statistically significant difference between the expected probability densities of the nonbranching crypts and the data for both groups A and B (group A, $\chi^2 = 59.1$, $dF = 58$, $P = 0.44$; group B, $\chi^2 = 41.1$, $dF = 39$, $P = 0.38$). The model predictions for the distribution of branching crypts of group A also were not significantly different from the data ($\chi^2 = 6.64$, $dF = 5$, $P = 0.25$). In contrast, for group B there was a statistically significant excess of small budding or branching crypts over that expected from the model for the measured range of a ($\chi^2 = 19.1$, $dF = 7$, $P < 0.008$). However, as a result of the small number of branching crypts observed, if only one of the smallest crypts judged to be branching on the basis of the crypt outlines was in fact not branching, then the model would not be inconsistent with the data at the 5% level ($\chi^2 = 13.4$, $dF = 7$, $P = 0.063$).

(f) Experiment 5: Search for Villus Production

A total of 71 pairs of villi surrounded by a single ring of crypts was found. Of these, 53 had one normal sized villus and one very small villus. The remaining 18 villus pairs had villi that were either roughly equal in size or had the smaller villus of intermediate size. The villus pairs were surrounded by 33 ± 0.82 ($\bar{x}$ ± SE) attached crypts (range 21–49), which is twice that found in Experiment 1 (which used the same tissue) for the mean number of crypts attached to randomly selected villi. 56 of the 2,345 crypts attached to villus pairs were branching crypts yielding a branching fraction of 0.0239 ± 0.0063 ($\bar{x}$ ± 95% confidence limits). This is about the same as the ratio of branching crypts estimated in Experiment 1 for the entire crypt population, indicating that these sites of paired villi are not sites of abnormal crypt production.

V. DISCUSSION

It has generally been assumed that the adult intestinal epithelium is in a steady state with cell production and loss being in balance. Our work shows, however, that unless special assumptions are made, the production and loss of crypt cells expected on the basis of current notions of crypt cell renewal does not admit a steady state. The observation that crypts are actively replicating makes it unnecessary and in fact incorrect to assume that the intestinal epithelium is in a steady state in the adult, although this may be a good approximation for some purposes (Bjerknes, 1986).

(a) Why a Crypt Cycle?

While it may seem surprising that the adult intestinal crypt population is not in a steady state, continuous crypt production is an empirical fact (Bjerknes, 1986).[4] The model of crypt growth presented here indicates that crypts can grow continuously without reaching a stable steady state. This results from a continuous expansion of the stem cell compartment. As the number of stem cells increases, the number of proliferating cells increases in direct proportion. As the number of cells in the crypt increases, the rate of cell loss increases both due to a greater force on the cells to leave the crypt and due to an increase in the perimeter of the waist. The rate of crypt growth is relatively slow since cell loss almost balances cell production. Nonetheless, this crypt growth driven by the expansion of the stem cell compartment provides a basis for crypt division since at some point the crypt becomes structurally unstable and division ensues. The model therefore suggests that the crypt cycle is an epiphenomenon of stem cell proliferation. The crypt replication time is a result of the interplay between cell production, cell loss, and crypt structural stability.

Alternatively, one might posit some feedback mechanism on the stem cell compartment of the crypt, permitting a steady-state crypt size. Introducing a form of feedback by fixing the growth fraction of the crypt did yield the possibility of a steady-state crypt size but was found, however, to result in excessively rapid crypt growth rates (Appendix C). Feedback is an extra assumption unwarranted by existing data. Our results indicate that the proposed crypt growth model without feedback fits the data on the rate of growth of crypts in both mouse jejunum and human sigmoid colon.

In applying the crypt growth model to the case of 30% resection in the mouse, the normal mouse jejunal parameter values were used, adjusted only to bring them into agreement with the observed changes in crypt size and replication time (Cheng et al., 1986*b*; Bjerknes and Cheng, 1981*d*). The ability of the model to account for the observed crypt growth rates without further fitting of the parameters indicates its generality. In agreement with experiment, the model does not require any increase in the number of transit divisions or reduction in the cell cycle time to obtain the measured growth rates after 30% resection (Bjerknes, 1981*d*; as discussed in Appendix A, the mean number of transit divisions is predicted by the model to be between 3.5 and 5).

The rate of expansion of the crypt population in mice with a doubling time of ~107 d, although rapid, is not inconsistent with the rate of increase in body weight (Bjerknes, 1986). In contrast, the crypt doubling time of 33 d after 30% resection in the mouse is sufficiently short that one must expect the crypt production rate in this case to eventually decrease. Further experimental investigation of the variation in crypt production rate with age of the mouse is required.

(b) All Crypts Are Cycling Asynchronously and Independently

The distribution of branching crypts both in random samples of crypts from over the epithelium (Experiment 1)

[4]It has been shown that the kinetic parameters of the intestinal epithelium are relatively stable for mice older than ~4 or 5 wk of age (Cheng and Bjerknes, 1985). We have therefore assumed that the data in Bjerknes (1986) obtained using young adult mice are representative of the adult.

and around individual villi (Experiment 2) was consistent with all crypts cycling asynchronously and independently. We found no evidence of noncycling crypts or clustering of cycling crypts. Thus it seems that all crypts are involved in crypt production, not just some specialized crypts or the crypts in specialized regions of the intestine. Although one would expect some correlation between sibling crypts since they presumably have roughly the same initial number of stem cells, noise in the process apparently is sufficient to quickly uncorrelate the cycling of crypts in a fashion similar to that which occurs in asynchronously cycling cell populations (Painter and Marr, 1968; Burnett-Hall and Waugh, 1967).

The asynchrony of crypt division implies that the crypt replication time is not a fixed constant. Suppose that the stem cell cycle time is, for simplicity, an exponentially distributed random variable with mean τ. Then the time for l divisions of a given stem cell is gamma distributed with the average time for l divisions being $l\tau$ with standard deviation $\sigma = \sqrt{l}\,\tau$ (see Frodesen et al., 1979). If T is the average crypt replication time, the average number of mitoses a stem cell undergoes before crypt division will therefore be $l = T/\tau$ so that the standard deviation of the crypt replication time would be $\sigma = \sqrt{T\tau}$. For $\tau = 13$ h and $T = 107$ d, the standard deviation is 7.6 d (i.e., 7% of the crypt cycle), which is already of the order of the period spent budding and bifurcating (see Eq. 21). The variance in crypt replication time would be further increased by asymmetry in the division process of the number of stem cells alloted to the daughter crypts.

A further possible contribution to the lack of synchrony between crypts surrounding a given villus (as demonstrated in Experiment 2) is if daughter crypts become associated with different villi so that adjacent crypts around a villus are not necessarily directly related. The results of Experiment 3 indicate that this is in fact often the case.

(c) Crypts Are Not a Homogeneous Population

The model of crypt growth and the cycling of crypts imply that crypts are continuously changing. Thus several crypt features vary significantly in the crypt population. This contrasts sharply with the classic view of the crypt as a steady-state structure with a fixed size, stem cell number, etc. Some of the quantities that vary are the following.

(*i*) Crypt size is not a constant. We found that crypts increase in volume by a factor of ~2 to 1 over the course of the crypt cycle (Experiment 4). Using an average cell size of 800 μm^3 for the mice of group A (see Appendix B), we found that jejunal crypts increased from roughly 325 to 775 cells during the crypt cycle (see Table IV). Direct cell counts of the number of cells per crypt made previously (Fig. 1 *a* of Cheng and Bjerknes, 1985) have a degree of variation comparable to that obtained here. This indicates that the variation in crypt volume observed here is not principally the result of variation in average cell size but rather the result of variation in the number of cells per crypt.

This observation suggests the need for a re-evaluation of the slow cut-off model of Cairnie et al. (1965) for the transition from proliferating to nonproliferating cells at the top of the proliferative zone of the crypt. Measurements of labeling index, mitotic index, and growth fraction as a function of cell position in the crypt actually determine, at each position, the averages of these quantities over the ensemble of crypt sizes. Since the absolute position of the top of the proliferative zone will likely vary with crypt size, such average measurements will tend to smooth out the apparent transition from actively proliferating to terminally differentiating cells, which occurs at the top of the proliferative zone. In particular, we propose that the inclusion of the effect of crypt size variability in the sharp cut-off model introduced but rejected by Cairnie et al. (1965) would be sufficient to explain the observed behavior of the average mitotic index with position. This would make unnecessary the assumption of a slow transition within the crypt between proliferating and nonproliferating cells.

(*ii*) The crypt growth model indicates that the number of stem cells per crypt is not a constant. Crypts on the verge of branching should have more stem cells than crypts at an earlier phase of the crypt cycle. This has important implications for drug and radiation studies of stem cell biology since it suggests the testable prediction that large crypts should be more difficult to kill than small ones in a given region of gut.

From Eqs. 16, A5, and A22, the probability distribution for the number of stem cells, s, in a randomly chosen crypt is

$$f(s)\,ds = 2s_0/s^2\,ds,$$

where s_0 is the number of stem cells in a crypt just after the completion of bifurcation. Assuming that the number of stem cells doubles during the crypt cycle, the number of stem cells in a crypt ranges from

$$s_0 = \bar{s}/(2 \ln 2) \tag{22}$$

to $\bar{s}/\ln 2$, where $\bar{s}$ is the average number of stem cells in a crypt. Given that $\bar{s} \simeq 15$ (Bjerknes and Cheng, 1981*c*; see also Potten and Hendry, 1983), the number of stem cells in a crypt varies from 11 to 22 over the course of the crypt cycle.

Alternatively, we can use the model of crypt growth to estimate $\bar{s}$ itself given c_0, the number of cycling cells in the smallest crypt, α, the average number of stem cells produced when a stem cell divides and m, the number of transit divisions that proliferating cells undergo enroute to the crypt top (see Appendix A). Substituting Eq. 22 into Eq. A24 yields

$$\bar{s} = 2 \ln 2\, c_0 \left(\frac{\alpha}{2}\right)^m.$$

Now c_0 and α can be estimated as described in this paper and m can be approximated using the method of Cleaver (1967), appropriately corrected for the geometry of the crypt base (see discussion at end of Appendix A). Values of m for mouse jejunum of between 2 and 3 in the literature (see Wright and Alison, 1984) are probably underestimates because the effect of crypt geometry has been neglected. Thus using the values of c_0 and α obtained here for mouse jejunum (see Tables I and V), the model predicts that the mean number of stem cells in a crypt, $\bar{s}$, is certainly less than 68 ($m = 2$), with a likely range being 8.6 ($m = 5$) to 24 ($m = 3.5$) stem cells (see Appendix A). Thus the model supports the smaller estimates of stem cell number (see discussion in Bjerknes, 1986).

(*iii*) The growth fraction of the crypt is not a constant. Variations in crypt growth fraction of roughly 5% were found in the model of crypt growth over the course of the crypt cycle (see Section IVa).

(*iv*) The rate of cell loss from a crypt is not constant. The total number of cells per unit time leaving the crypt roughly doubles over the course of the crypt cycle (assuming the parameter values shown in Table I and assuming that the number of cells in a crypt doubles over the crypt cycle). For the normal mouse jejunum this rate varies roughly from 11 cells/h to 30 cells/h (using n_i and n_f in Table I; see Eq. 8).

From this point of view, measured variances of these quantities are principally due to their intrinsic variation in the crypt population.

(d) The Role of Crypt Size in the Crypt Cycle

We found that the distribution of crypt volumes is consistent with the notion that most crypts steadily grow until they become large enough to divide. The two smaller crypts in turn grow and divide and so on (Experiment 4). As expected then, bifurcating and nonbifurcating crypts do not form two distinct populations with disparate size distributions; rather, the nonbifurcating crypts span a range of sizes that overlaps that of the bifurcating crypts, indicating that nonbifurcating and bifurcating crypts constitute a single continuous size distribution (see Figs. 7 and 8). Bifurcating crypts tend on the average to be larger than nonbifurcating crypts. These findings implicate the size of the crypt as a factor in the division process and suggest the possibility that mechanical instability triggers crypt bifurcation. Although the size of the crypt is correlated with the onset of division, it is clear that the relationship is subtle since after resection the maximum crypt size apparently increases. An elucidation of the mechanical factors responsible for determining crypt size should give insight into the triggering of the process of crypt bifurcation.

TABLE V
CELL AND CRYPT PRODUCTION PARAMETERS*

	τ	T	α	k	k'
	h	d		h^{-1}	h^{-1}
Mouse jejunum	13	107	1.0035	2.71×10^{-4}	0.0768
Human sigmoid colon	72	4380	1.000475	6.58×10^{-6}	0.0139
Mouse jejunum after 30% resection	13	33	1.0114	8.75×10^{-4}	0.0765

*Definition and manner of determination of these parameters explained in Appendix A.

(e) Villus Production

In this paper we reported evidence suggestive of villus production in the adult mouse. The proliferative compartment of the villus is made up of the crypts surrounding it. As the number of crypts around a villus increases through crypt replication, the size of the villus continuously grows (Cheng and Bjerknes, 1985). The results of Experiment 5 indicate that when the number of crypts around a villus is roughly double the average number and the villus has grown sufficiently, the production of a new villus may occur. The apparent instability of the larger villus structure appears again to demonstrate a competition between cell production and structural stability. Sites of villus production are apparently not abnormal since no significant increase in the crypt branching rate was found at these sites. In light of the demonstrated production of crypts, it is unlikely that the pairs of villi we have observed are the result of villus merging.

Given that villi are being produced in the adult, the simplest conclusion would be that the villus population is increasing. Contrary data in the rat have been reported (see Wright and Alison, 1984); however, given the apparently small rate of villus production, such direct measurements of the total number of villi are probably not sufficiently precise to reveal the supposed small changes in the villus population.

VI. CONCLUSIONS

(a) Most if not all crypts of the adult mouse intestinal epithelium cycle asynchronously and independently. The crypt population is not in a steady state in the adult; rather it is slowly increasing. *(b)* A steady-state crypt size is theoretically unjustified. A steady-state crypt size is not a necessary result of a model of crypt growth constructed using current understanding of crypt cell kinetics, which can explain the data on the growth of crypts in the mouse both before and after resection and in the human. Crypt volume is predicted to grow roughly linearly in time over the measured crypt cycle times and range of sizes. *(c)* Crypt bifurcation is an epiphenomenon of stem cell proliferation with crypts bifurcating when they approximately double their original volume. The occurrence of crypt bifurcation (and thus of a crypt cycle) obviates the need to maintain a steady-state crypt size (with the associated special feedback mechanisms) to achieve a reasonable range of crypt sizes. *(d)* Crypt production leads to a steady

increase in villus size. This in turn leads to active production of villi in the adult mouse.

APPENDIX A

Cell Production in the Crypt

For simplicity we use a discrete, deterministic model (see Eisen, 1979). Denoting time by t and the cell cycle time (assumed fixed) by τ, we define discrete time by

$$i = t/\tau, \tag{A1}$$

where $i = 0, 1, 2, \ldots$ We identify three subpopulations or compartments of the total population of cells in a crypt: the stem cells, the remaining proliferating cells that will each undergo a total of m transit divisions enroute towards the mouth of the crypt, and lastly the noncycling cells which are completing their terminal differentiation. Let the number of cells in each compartment be denoted as follows: s cells in the stem cell compartment, p in the proliferative compartment, and q in the noncycling compartment. It is convenient to further subdivide the proliferative compartment into m subpopulations. Cells leaving the stem cell compartment enter the first proliferative compartment. The number of cells in this compartment is denoted by p_1. Upon dividing, the p_1 cells and their daughters enter the next proliferative compartment denoted p_2. This continues until the mth proliferative compartment is reached. Upon division, the p_m cells in this compartment and their daughters enter the q compartment. With these definitions,

$$p = \sum_{j-1}^{m} p_j, \tag{A2}$$

$$c = s + p \tag{A3}$$

and

$$n = s + p + q, \tag{A4}$$

where c is the total number of cycling cells and n is the total number of cells.

Consider the stem cell compartment. Let α be the average number of stem cells produced when a stem cell divides ($1 < \alpha < 2$). Denoting the initial number of stem cells by s_o, then the number of stem cells at time i is

$$s = s_o \alpha^i \tag{A5}$$

(see Eisen, 1979). Since each stem cell at time $i - 1$ becomes 2 cells at time i, the number of cells leaving the stem cell compartment at time i is

$$2s_o\alpha^{i-1} - s_o\alpha^i = s_o\alpha^{i-1}(2 - \alpha). \tag{A6}$$

Let $p_j(0)$ be the initial number of proliferating cells in each of the respective proliferative compartments. Since the number of cells in the p_1 compartment at time i is just the number of cells leaving the stem cell compartment, we have

$$p_1(i) = \begin{cases} p_1(0), i = 0 \\ s_o\alpha^{i-1}(2 - \alpha), i > 0. \end{cases} \tag{A7}$$

(see Eq. A6).

For p_2, the number of cells in this compartment at time $i > 0$ is simply twice p_1 at $i - 1$. Therefore,

$$p_2(i) = \begin{cases} p_2(0), i = 0 \\ 2p_1(0), i = 1 \\ 2p_1(i - 1), i > 1. \end{cases} \tag{A8}$$

In a similar way we obtain for the proliferative compartments p_j, $j = 2, 3, \ldots, m$,

$$p_j(i) = \begin{cases} p_j(0), i = 0 \\ 2^i p_{j-1}(0), 0 < i \le j - 1 \\ 2^{j-1}p_1(i - [j - 1]), i > j - 1. \end{cases} \tag{A9}$$

Using these expressions and Eqs. A2 and A5, we obtain for $i \ge m$[5]

$$\begin{aligned} p(i) &= \sum_{j-1}^{m} p_j(i) \\ &= s_o \alpha^i \left[\left(\frac{2}{\alpha}\right)^m - 1\right]. \end{aligned} \tag{A10}$$

Therefore,

$$c(i) = s_o \alpha^i \left(\frac{2}{\alpha}\right)^m \tag{A11}$$

(see Eq. A3).

Finally the q compartment, starting with the initial population q_o, increases at time i by twice p_m at $i - 1$. Therefore,

$$q(i) = \begin{cases} q_o, i = 0 \\ q_o + \sum_{i'-1}^{i} 2p_m(i' - 1), i > 0. \end{cases} \tag{A12}$$

Substituting Eqs. A7 and A9 into A12 and doing the sum gives for $i \ge m$,

$$\begin{aligned} q(i) &= q_o + \sum_{h-o}^{m-1} 2 \times 2^h p_{m-h}(0) \\ &\quad + \sum_{h-m}^{i-1} 2 \times 2^{m-1} p_1(h - m + 1) \\ &= q_o + \sum_{j-1}^{m} 2^{m-(j-1)} p_j(0) \\ &\quad + \frac{(2 - \alpha)}{(\alpha - 1)} s_o 2^m (\alpha^{i-m} - 1). \end{aligned} \tag{A13}$$

We have found then that for $t \ge m\tau$ (recall Eq. A1),

$$c(t) = s_o \left(\frac{2}{\alpha}\right)^m e^{t \ln \alpha/\tau} \tag{A14}$$

and

$$q(t) = \frac{(2 - \alpha)}{(\alpha - 1)} s_o \left(\frac{2}{\alpha}\right)^m (e^{t \ln \alpha/\tau} - e^{m \ln \alpha}) + Q, \tag{A15}$$

where Q is a constant.

Therefore,

$$\frac{dc}{dt} = kc \tag{1}$$

[5]Since $m\tau$ is small compared with the crypt replication time, we may restrict ourselves to long time behavior.

and

$$\frac{dq}{dt} = k\rho c \tag{2}$$

where

$$k = \frac{\ln \alpha}{\tau} \tag{A16}$$

and

$$\rho = \frac{(2-\alpha)}{(\alpha - 1)}. \tag{A17}$$

Hence (using Eqs. A3 and A4),

$$\frac{dn}{dt} = \frac{dc}{dt} + \frac{dq}{dt} = k'c \tag{A18}$$

where

$$k' = k(\rho + 1) = k/(\alpha - 1). \tag{A19}$$

We assume that the stem cell population doubles in the crypt replication time T. From Eq. A5 we have that

$$\frac{ds}{dt} = ks, \tag{A20}$$

where k is given by Eq. A16. In terms of the time for the stem cell population to double, T,

$$k = \frac{\ln 2}{T}. \tag{A21}$$

Thus

$$\frac{\ln 2}{T} = \frac{ln\alpha}{\tau}, \tag{A22}$$

which implies that

$$\alpha = 2^{\tau/T}.$$

This means that

$$k' = \frac{\ln 2}{T(2^{\tau/T} - 1)}, \tag{A23}$$

which is relatively insensitive to changes in T for fixed τ (if $T \gg \tau$). As $T \to \infty$, $k' \to 1/\tau$.

Table V lists the values used for τ, T, α, k, and k' for normal mouse jejunum, for mouse jejunum 3 wk after 30% resection, and for human sigmoid colon. For the mouse, a cell cycle time of $\tau = 13$ h (cf. Cheng and Bjerknes, 1983; Wright and Alison, 1984) was used. The estimated crypt replication times were $T = 107$ d = 2,568 h (Bjerknes, 1986) in normal jejunum and $T = 33$ d (Cheng et al., 1986*b*) in resected epithelium. For the human sigmoid colon we used $\tau = 3$ d and $T = 12$ yr = 4,380 d (cf., Appendix 1 of Cheng et al., 1986*a*).

Frome Eq. A11, we have that

$$c_0 = s_0\left(\frac{2}{\alpha}\right)^m, \tag{A24}$$

where c_0 and s_0 are the number of cycling and stem cells, respectively, for the smallest sized crypts. Assuming that the average number of stem cells in a crypt, $\bar{s}$, lies between 10 and 20 in normal mouse jejunum (Bjerknes and Cheng, 1981*c*; see also Potten and Hendry, 1983), then s_0 is given by Eq. 22 to lie in the range of roughly 7–14 stem cells. Substituting into Eq. A24 these values of s_0 and the values of c_0 and α for the mouse given in Tables I and V, we find that m has a value in the range 3.8–4.8. Assuming that the ratio c_0/s_0 is about the same after resection as before, we find using Eq. A24 that 3 wk after 30% resection m is somewhere in the range 3.9–4.9. We conclude, therefore, that the number of transit divisions is somewhere between 3.5 and 5. Estimates in the literature of between 2 and 3 transit divisions (see Cleaver, 1967; Wright and Alison, 1984; Bjerknes and Cheng, 1981*d*) are likely incorrect because the decrease in the circumference of the cross-section of the crypt (and hence in the number of cell columns) as one moves towards the base of the crypt was neglected in the computations of m.

APPENDIX B

Parameter Estimation for the Crypt Growth Model

Published data on the crypt replication time, T, and on the rate of loss of cells from a crypt whose stem cells have been killed were used in the estimation of the parameters s and r (see Eq. 10) as follows. We assume that s and r are chosen so that the crypt will grow from its smallest number of cells n_i to its largest number (just before branching) n_f in the time T. This yields possible pairs of s and r values. To determine a specific pair of s and r we then choose the pair that agrees with the existing data on the rate of loss of cells from a crypt whose stem cells have been killed.

Various drugs or irradiation may be used to kill proliferating cells. If sufficient doses are given, entire crypts can be lost (see Figs. 21.5B and 23.3C of Wright and Alison, 1984). Over the time scale of crypt regeneration, the loss of crypts is rapid so that the time taken to reach minimum density simply corresponds to the time necessary for the largest crypts to empty. Modeling of crypt loss is hampered by the lack of quantitative data on the range of crypt sizes involved in a given experiment, on the number of cells killed, on the number of cells lost to the lumen, and on the amount of cell production that continues after cytotoxic insult. To make rough estimates of the rate at which crypts disappear, we turn to the irradiation data.

For a crypt irradiated strongly enough that it eventually disappears, the following assumptions are made: *(a)* All stem cells are killed; *(b)* Largest crypts disappear in 2 d (Wright and Alison, 1984); *(c)* No significant mitotic activity over period of crypt loss (cf. Sherman and Quastler, 1960; Fig. 3.5 of Potten et al., 1983); *(d)* Accumulation of large G_2 cells in crypt and irradiation generally do not severely change migration rate (see Wright and Alison, 1984); *(e)* A crypt is classified as having disappeared when all but the Paneth cells have emptied out of the growth zone, i.e., when the number of cells in the growth zone is reduced to ~20 (Bjerknes and Cheng, 1981*a*); *(f)* The number of cells killed by the irradiation or lost to the lumen ranges from just 5% of the total number of cells in the crypt (Potten et al., 1978) (this corresponds to roughly the number of stem cells in the crypt) to a conservative upper bound of 25% of the total number of cells in the crypt; *(g)* Killed cells are lost to the lumen or phagocytosed immediately and are, therefore, not lost by migration out of the crypt.

Under these assumptions, crypt loss is modeled as follows. In Eq. 10, c_0 is set to zero. The equation is numerically solved with the initial number of cells being the number of cells in the largest crypt n_f less the number of cells killed. The parameters s and r are then chosen so that after 2 d only 20 cells are left in the growth zone. That pair of values for s and r that also satisfies the constraint on the rate of normal crypt growth, is the value of s and r presented in Table I. The ranges of s and r given in the table are the result of assuming that the initial number of cells killed ranges from 5–25% of the total number of cells in the crypt.

In Secion II, a number of additional parameters have been introduced. Estimates of their values are also listed in Table I. The way in which these estimates were made is now briefly discussed. The average volume of a crypt cell $\bar{v}$ introduced in Section IIc was obtained from $\bar{v} = \bar{V}/\bar{n}_{TOT}$,

where $\bar{V}$ is a representative average crypt volume measured in Experiment 4 and $\bar{n}_{TOT}$ is an estimate of the average total number of cells in a crypt. For the mouse we used $\bar{V} = 4 \times 10^5\ \mu m^3$ (see Fig. 7) and $\bar{n} = 500$ (see Table 1 of Cheng and Bjerknes, 1983, and Cheng and Bjerknes, 1985) so that $\bar{v}$ for group A mice is 800 μm^3. This is consistent with the observed linear dimensions of mid-crypt columnar cells (see Fig. 7 of Cheng and Leblond, 1974; Table 3 of Bjerknes and Cheng, 1981*a*). With this value of $\bar{v}$, the total number of cells in the crypts of group A ranges from 325 to 775 cells. As representative values, we have assumed that the crypt growth fraction is 60% (Wright and Alison, 1984; Table 2 of Cheng and Bjerknes, 1983) and that ⅔ of the total number of cells in a crypt are in the growth zone (Table 2 of Bjerknes and Cheng, 1981*d*). This means that the growth fraction below the waist, γ, is 90% and that the number of cells in the growth zone ranges from $n_i = 217$ to $n_f = 517$. c_o is obtained using the equation $c_o = \gamma n_i$, so that $c_o = 195$.

Rough data on the rate of crypt branching are now available for the human sigmoid colon (Cheng et al., 1986*a*). The mean size of a colonic crypt is ~2,500 cells (Cheng et al., 1984). Based on the rough location of the waist in colonic crypts (see Fig. 1 of Cheng et al., 1984), we have assumed that the growth zone comprises ~50% of the crypt and its associated surface epithelium. Thus, the average number of cells in the growth zone of the colonic crypt is ~1,200. Assuming a relative range of crypt sizes about the mean comparable to that found in mouse jejunum, we obtain $n_i = 600$ and $n_f = 1{,}800$. The growth fraction of colonic epithelium in the mouse has been found to be 0.31 (Cheng and Bjerknes, 1982). Assuming a similar value for human colon, the growth fraction of the growth zone in human colon would be roughly $\gamma = 0.6$. Since data on the rate of crypt loss after irradiation similar to that for the mouse jejunum was unavailable, we simply assumed that r representing the ratio ϕ/σ was the same as in the mouse and chose s so that the crypt would grow from n_i to n_f in the doubling time T.

APPENDIX C

Crypt Growth with Constant Growth Fraction

In the model we have presented, the growth fraction is permitted to change. If the growth fraction was fixed by some means, then we could assume that in the absence of cell loss

$$\frac{dn}{dt} = k^* n,$$

where

$$k^* = \frac{\ln(1+\gamma)}{\tau},$$

with γ being the fixed growth fraction. Incorporating the loss of cells through the top of the growth zone as before gives

$$\frac{dn}{dt} = k^* n - \Gamma n^{1/3}(\sigma n + \phi)$$

$$= \frac{k^*}{s^*}(-n^{4/3} + s^* n - r n^{1/3}),$$

where $s^* = k^*/\sigma\Gamma$ and $r = \phi/\sigma$ as before (see Eq. 12).

Since crypts are growing, we require that dn/dt be positive for some range of positive n. This is assured if

$$\frac{r}{s^*} < \frac{4}{27},$$

in which case a plot of dn/dt as a function of n is of the form shown in Fig. 9. The points n_1 and n_2 labeled in Fig. 9 are given by

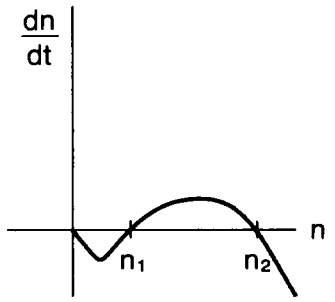

FIGURE 9 Sketch of dn/dt vs. n as given by the equation for dn/dt in Appendix C when $r/s^{*3} < 4/27$ (see Appendix C for parameter definitions).

$$n_1 = \left(\frac{s^*}{3}\right)^3 \left[2\cos\left(\frac{\theta}{3} + \frac{4\pi}{3}\right) + 1\right]^3$$

and

$$n_1 = \left(\frac{s^*}{3}\right)^3 \left[2\cos\frac{\theta}{3} + 1\right]^3,$$

where

$$\cos\theta = 1 - \frac{r}{2}\left(\frac{3}{s^*}\right)^3$$

and $0 < r < 4(s^*/3)^3$ (see above). Crypts with less than n_1 cells empty out, whereas, those with between n_1 and n_2 cells grow in size. In this model, crypts with n_2 cells are in stable equilibrium. This contrasts with the previous model, which did not possess a stable equilibrium. It is biologically reasonable to assume that n_1 is the number of cells corresponding to about one stem cell left in the crypt. With this choice, s^* and r could not be chosen so that the crypts would grow in size from the smallest measured crypt n_i to the largest n_f in the time necessary for crypt replication without most of the crypt cycle being spent near n_f, which gives a volume distribution inconsistent with the data. Instead, reasonable choices of s^* and r yield growth rates of the order of five times too fast (comparable to crypt replication times after resection). Fixing the growth fraction, therefore, leads to excessive growth rates.

We are grateful to R. Kuk for technical assistance and to P. Topham for help in preparing the manuscript. Thanks also to J. Winslow for his comments on the paper.

One of us (J. Totafurno) gratefully acknowledges the support of a Medical Research Council Postdoctoral Fellowship. This work was funded by grants from the Medical Research Council of Canada and the Canadian Foundation for Ileitis and Colitis.

Received for publication 2 October 1986 and in final form 18 March 1987.

REFERENCES

Abramowitz, M., and I. A. Stegun. 1965. Handbook of Mathematical Functions. Dover Publications, Inc., New York.

Bjerknes, M. 1986. A test of the stochastic theory of stem cell differentiation. *Biophys. J.* 49:1223–1227.

Bjerknes, M., and H. Cheng. 1981*a*. The stem cell zone of the small intestinal epithelium. I. Evidence from Paneth cells in the adult mouse. *Am. J. Anat.* 160:51–63.

Bjerknes, M., and H. Cheng. 1981*b*. The stem cell zone of the small

intestinal epithelium. II. Evidence from Paneth cells in the newborn mouse. *Am. J. Anat.*160:65–75.

Bjerknes, M., and H. Cheng. 1981*c*. The stem cell zone of the small intestinal epithelium. III. Evidence from columnar, enteroendocrine, and mucous cells in the adult mouse. *Am. J. Anat.*160:77–91.

Bjerknes, M., and H. Cheng. 1981*d*. The stem cell zone of the small intestinal epithelium. IV. Effects of resecting 30% of the small intestine. *Am. J. Anat.* 160:93–103.

Bjerknes, M., and H. Cheng. 1981*e*. Methods for the isolation of intact epithelium from the mouse intestine. *Anat. Rec.* 199:565–574.

Bjerknes, M., and H. Cheng. 1985. Mucous cells and cell migration in the mouse duodenal epithelium. *Anat. Rec.* 212:69–73.

Burnett-Hall, D. G., and W. A. O'N. Waugh. 1967. Indices of synchrony in cellular cultures. *Biometrics.* 23:693–716.

Cairnie, A. B., L. F. Lamerton, and G. G. Steel. 1965. Cell proliferation studies in the intestinal epithelium of the rat. *Exp. Cell Res.* 39:539–553.

Cairnie, A. B., and B. H. Millen. 1975. Fission of crypts in the small intestine of the irradiated mouse. *Cell Tissue Kinet.* 8:189–196.

Cheng, H., and M. Bjerknes. 1982. Whole population cell kinetics of mouse duodenal, jejunal, ileal, and colonic epithelia as determined by radioautography and flow cytometry. *Anat. Rec.* 203:251–264.

Cheng, H., and M. Bjerknes. 1983. Cell production in mouse intestinal epithelium measured by stathmokinetic flow cytometry and Coulter particle counting. *Anat. Rec.* 207:427–434.

Cheng, H., and M. Bjerknes. 1985. Whole population cell kinetics and postnatal development of the mouse intestinal epithelium. *Anat. Rec.* 211:420–426.

Cheng, H., and C. P. Leblond. 1974. Origin, differentiation and renewal of the four main epithelial cell types in the mouse small intestine. I. Columnar cell. *Am. J. Anat.* 141:461–480.

Cheng, H., M. Bjerknes, and J. Amar. 1984. Methods for the determination of epithelial cell kinetic parameters of human colonic epithelium isolated from surgical and biopsy specimens. *Gastroenterology.* 86:78–85.

Cheng, H., M. Bjerknes, J. Amar, and G. Gardiner. 1986*a*. Crypt production in normal and diseased human colonic epithelium. *Anat. Rec.* 216:44–48.

Cheng, H., C. McCulloch, and M. Bjerknes. 1986*b*. Effects of 30% intestinal resection on whole population cell kinetics of mouse intestinal epithelium. *Anat. Rec.* 215:35–41.

Cleaver, J. E. 1967. Thymidine Metabolism and Cell Kinetics. John Wiley & Sons, Inc., New York. 211–212.

Eisen, M. 1979. Mathematical models in cell biology and cancer chemotherapy. *Lect. Notes Biomath.* Chap. II. 30.

Fisher, R. A. 1970. Statistical Methods for Research Workers. Oliver and Boyd, Edinburgh. 99–100.

Frodesen, A. G., O. Skjeggestad, and H. Tofte. 1979. Probability and Statistics in Particle Physics. Columbia University Press, Irvington-on-Hudson, New York. 95–98.

Maskens, A. P., and R. M. Dujardin-Loits. 1981. Kinetics of tissue proliferation in colorectal mucosa during post-natal growth. *Cell Tissue Kinet.* 14:467–477.

O'Connor, T. M. 1966. Cell dynamics in the intestine of the mouse from late fetal life to maturity. *Am. J. Anat.* 118:525–536.

Painter, P. R., and A. G. Marr. 1968. Mathematics of microbial populations. *Ann. Rev. Microbiol.* 22:519–548.

Potten, C. S., S. E. Al-Barwari, and J. Searle. 1978. Differential radiation response amongst proliferating epithelial cells. *Cell Tissue Kinet.* 11:149–160.

Potten, C. S., and J. H. Hendry. 1983. Stem cells in murine small intestine. *In* Stem Cells. C. S. Potten, editor. Churchill Livingstone, New York. 155–199.

Potten, C. S., J. H. Hendry, J. V. Moore, and S. Chwalinski. 1983. Cytotoxic effects in gastro-intestinal epithelium (as exemplified by small intestine). *In* Cytotoxic Insult to Tissue. C. S. Potten and J. H. Hendry, editors. Churchill Livingstone Inc., New York. 105–152.

Sherman, F. G., and H. Quastler. 1960. DNA synthesis in irradiated intestinal epithelium. *Exp. Cell Res.* 19:343–360.

Sokal, R. R., and F. J. Rohlf. 1981. Biometry. 2nd ed. W. H. Freeman & Co., Publishers, San Francisco. 716–721.

Steel, G. G. 1968. Cell loss from experimental tumours. *Cell Tissue Kinet.* 1:193–207.

Wright, N., and M. Alison. 1984. The Biology of Epithelial Cell Populations. Vol. 2. Clarendon Press, Oxford.